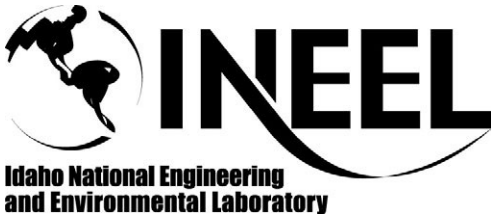

INEEL/CON-04-02467
PREPRINT

Microstructure And Mechanical Properties Of Spray-Formed H13 Steel Tooling

Yaojun Lin
Kevin M. McHugh
Young-Soo Park
Yizhang Zhou
Enrique J. Lavernia

February 13-17, 2005

134th Annual Meeting And Exhibition – The Minerals, Metals & Materials Society (TMS) 2005

MICROSTRUCTURE AND MECHANICAL PROPERTIES OF SPRAY-FORMED H13 STEEL TOOLING

[1]Yaojun Lin, [2]Kevin M. McHugh, [1]Young-Soo Park,
[1]Yizhang Zhou, and [1]Enrique J. Lavernia

[1]Department of Chemical Engineering and Materials Science,
University of California, Davis, CA 95616-5294, USA

[2]Industrial and Material Technologies Department,
Idaho National Engineering and Environmental Laboratory, Idaho Falls, ID 83415, USA

Key words: Spray-formed tooling; H13 steel; Process development

Abstract

This paper presents results on the microstructure and hardness of spray-formed H13 (Fe-0.40C-5.00Cr-1.10V-1.30Mo (wt%)) tooling. There is very low porosity in both as-spray formed samples and aged samples. The microstructure in the as-spray-formed sample is characterized by primary carbides, acicular lower bainite, and a small amount of martensite and retained austenite. Spray formed and aged tooling H13 has higher hardness values than those of H13 in conventional tooling. The experimental results of microstructures and hardness are rationalized on the basis of numerical analysis of cooling during processing of spray-formed tooling.

Introduction

Spray forming has been the topic of numerous studies over the past few decades [1]; more recently, this technology has been successfully implemented for the fabrication of molds and dies [2, 3]. During this approach, atomized droplets are directed towards a pre-designed pattern where they accurately capture features of the pattern during solidification to form the desired mold or die. Compared with conventional techniques for mold/die production, a series of machining, grinding, and polishing steps can be eliminated in spray-formed tooling. Furthermore, as compared with the heat treatment operations in conventional mold/die fabrication techniques, long-time annealing can be avoided due to the formation of a homogeneous and macrosegregation-free microstructure that is characteristic of as-spray formed materials [3, 4]. Moreover, rapid solidification during spray forming may suppress carbide precipitation and growth, allowing tool steels to be artificially aged directly from the as spray formed state to obtain the final mold/die products. In contrast, conventional austenitization/quench/temper heat treatment is required in conventional mold/die-making techniques. Therefore, spray-formed tooling will save energy, production time and costs, and avoid mold/die distortion during heat treatment. This paper reports on an investigation of the microstructures (e.g., porosity and phases) and hardness of spray-formed H13 tooling. The microstructures and hardness obtained in experiments were rationalized on the basis of numerical simulation results.

Experimental

Commercial H13 steel (Fe-0.40C-5.00Cr-1.10V-1.30Mo (wt%)) and nitrogen were used in the spray-formed tooling experiment reported in the present study. A schematic of the

approach [5] is shown in Fig. 1. During processing of spray-formed tooling, a preheated substrate was adopted and experimental conditions are listed as follows: atomization pressure 0.14 MPa, molten metal superheat 100 °C, metal flow rate 45.4 g/s, gas flow rate 5.8 g/s, deposition distance 254 mm, and average growth rate of the deposit 0.24 mm/s. The samples investigated in the present study were sectioned from the three positions of the spray-formed materials: the deposit/substrate interfaces, central regions and exposed surfaces. Some samples were artificially aged under various conditions (Table II). Analysis was performed on the as-deposited samples and the aged samples using: i) optical microscope (OM) observation to determine porosity using Analysis^{TM} software, ii) OM, scanning electron microscope (SEM), transmission electron microscope (TEM) observation to examine microstructures, and iii) hardness testing.

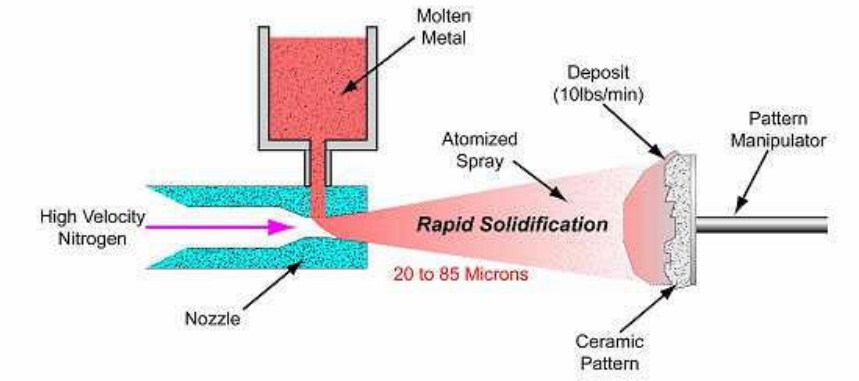

Fig. 1: Schematic of spray-formed tooling [5].

Table I: Thermal and physical properties of H13 and ceramic substrate

Materials	Property	Value	Ref.
H13	Thermal conductivity	28 W/mK	6
	Density	7000 kg/m^3	
	Specific heat	447 J/kgK	
	Latent heat of fusion	2.8×10^5 J/kg	
	Liquidus temperature	1454 °C	7
	Solidus temperature	1315 °C	
	Equilibrium distribution coefficient	0.35	
Ceramic	Thermal conductivity	1 W/mK	6
	Density	1700 kg/m^3	
	Specific heat	900 J/kgK	

Numerical Modeling

The processing of tooling by spray forming can be divided into two distinct but closely related stages: first, flight, and then, deposition. During flight, the thermal energy of the atomized droplets is extracted via convection heat transfer between the droplets and the atomization gas and via radiation heat transfer. During flight, the temperatures and the solid fractions of individual droplets can be calculated using an equation of energy conservation [8]. At the deposition distance, by combining the calculated temperatures and solid fractions of individual droplets with the droplet-size distribution predicted using the Lubanska correlation [9], the average temperature and solid fraction of incoming droplets at impact can be evaluated using the enthalpy method [10], and used as input data for the calculation of the cooling process in the deposition stage.

During deposition, heat conduction within the spray-formed material can be assumed to be 1-D along the thickness of the spray-formed material because the thickness of molds/dies is usually much smaller than their width/length. The buildup of the deposit occurs via discrete deposition of individual droplets [11], i.e., there exists a time interval between two groups of droplets that successively arrive at the previously deposited material's surface. Accordingly, a 1-D Fourier's equation is used to deal with heat conduction within the deposit during a time interval. At the end of this time interval, a new group of droplets is incorporated to the previously deposited material to generate a new deposit. Fourier's equation is then implemented to compute heat conduction within the new deposit. In the present study, the alternating-direction explicit (ADE) method is used to discretize Fourier's equation as described in [11]. The assumption of 1-D heat transfer along the thickness and the ADE method are also applicable to the pattern (substrate) due to the much smaller thickness than the width and length, in order to calculate the pattern's temperature required for the calculation of the cooling process within the deposit. In the calculations that follow, the relevant thermal and physical properties of H13 and of ceramic substrate are listed in Table I.

Results and Discussion

Experimental Results

Table II shows the measured porosity in spray-formed H13 samples sectioned from different positions in the deposit and processed under different conditions. In all of the samples, porosity is lower than 1%.

Table II: Porosity in various spray-formed H13 steel samples.

Sample location	Sample no.	Heat treatment	Porosity (vol.%)
Deposit/ Substrate Interface	1	As-deposited	0.10
	2	500 °C × 2 hours	0.12
	3	630 °C × (2+2) hours	0.71
Exposed Surface	4	As-deposited	0.05
Middle	5	1052 °C (air quenching) & 593 °C × (2+2) hours	0.55

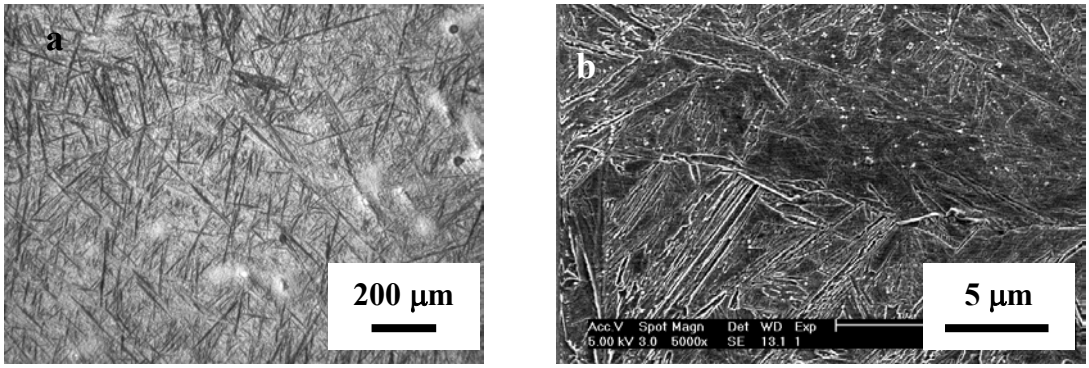

Fig. 2: Microstructures of as-deposited H13 (No. 4 sample): (a) OM, and (b) SEM.

In Fig. 2a, the OM image of as-spray-formed H13 (No. 4 sample) exhibits dark acicular microstructures separated by the bright regions. In the SEM image of No. 4 sample (Fig. 2b), proeutectoid carbides can be observed (white particles). The TEM images of dark acicular microstructures in Fig. 2a exhibit typical lower bainite morphology (Fig. 3): bainitic ferrite (labeled "A"), vanadium-rich MC-type carbides between bainitic ferrite (labeled "B") and vanadium-rich MC-type carbides inside bainitic ferrite (labeled "C"). Fig. 4a is the TEM bright field image of the bright regions in Fig. 2a. Indexing of the diffraction pattern in Fig. 4b (γ-Fe

diffraction from [001] zone axis) indicates the existence of retained austenite. This fact also implies that martensite may exist in the No. 4 H13 sample.

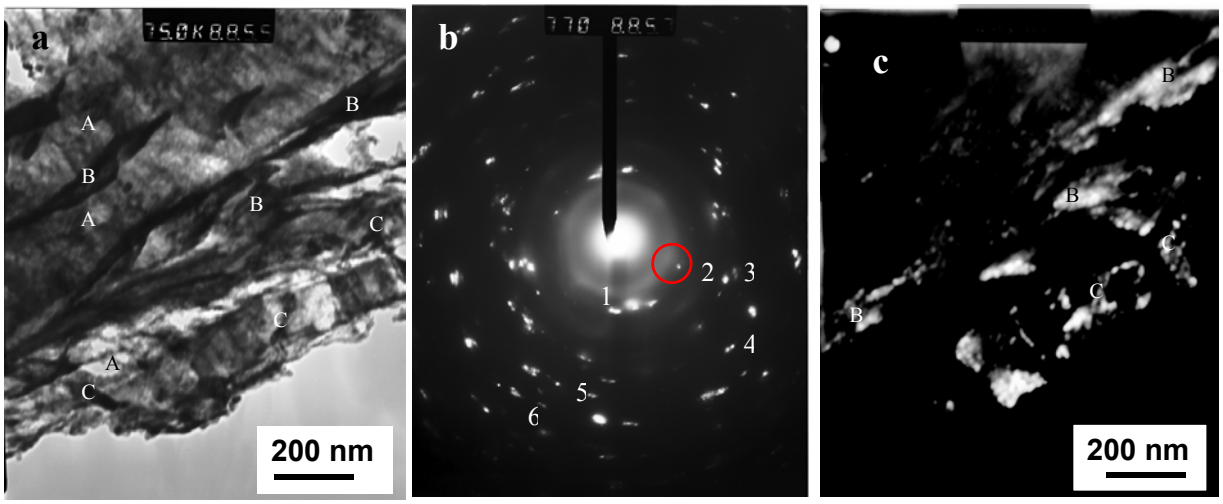

Fig. 3: TEM images of dark acicular microstructures in Fig. 2a: (a) bright field image, (b) corresponding selected area diffraction (SAD) pattern of vanadium-rich MC type carbides characterized by the traces of the rings: 1{111}, 2{022}, 3{113}, 4{222}, 5{004} and 6{133}, and (c) dark field image from the circled spot ({111} plane) in the diffraction pattern.

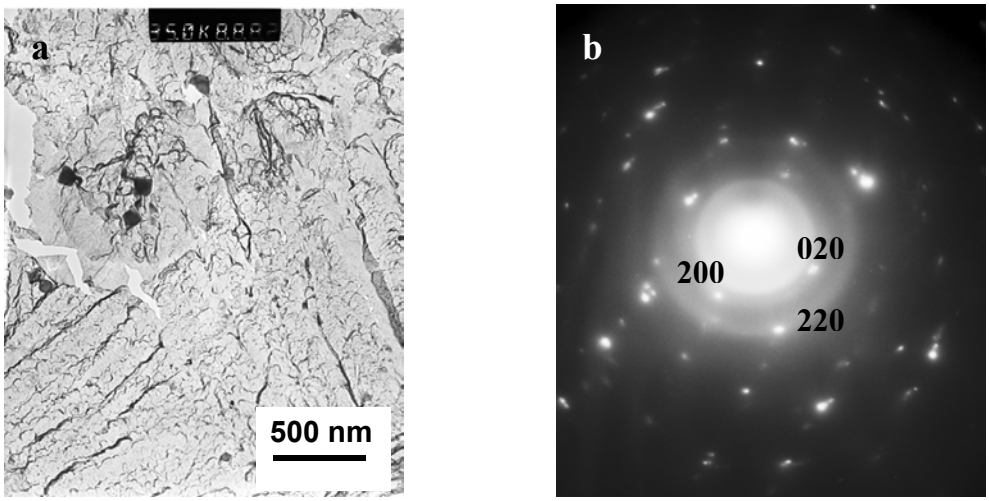

Fig. 4: TEM images of the bright regions in Fig. 2a: (a) bright field image, (b) corresponding SAD pattern: γ-Fe diffraction from [001] zone axis.

Table III: The hardness of spray-formed H13

Spray-formed H13				Conventional air quenching of H13 [12]
Sample Location	Sample No.	Heat Treatment	Hardness (HRC)	Hardness (HRC)
Deposit/Substrate Interface	1	As-deposited	55.2	50.0
	2	500 °C × 2 hours	56.6	53.3
	3	630 °C × (2+2) hours	40.3	39.6
Exposed Surface	4	As-deposited	54.3	50.0

Table III compares the hardness values of spray-formed H13 and those of H13 processed via conventional heat treatments. Under the same aging condition, the hardness

value of spray-formed H13 is higher than that of conventional H13. It is noted that, during conventional heat treatment, H13 is austenitized at 1010 °C and air quenched.

Simulation Results and Discussion

Fig. 5 shows the calculated temperature as a function of time at deposit/substrate interface, half thickness of the deposited material, and the exposed surface of the deposited material. Results indicate that during spray forming, liquid phase is present throughout the entire thickness of the deposited material. By assuming equilibrium for the simulation in Fig. 5, an estimation of liquid fraction is obtained (Fig. 6). In Fig. 6, it is shown that throughout the entire thickness of the deposited material (e.g., at deposit/substrate interface, half thickness, and the exposed surface), the maximum liquid fraction is above 20%, which is required for complete removal of porosity [13]. The liquid fraction exists for 30 to 480s. These results support the observed very low porosity values in Table II.

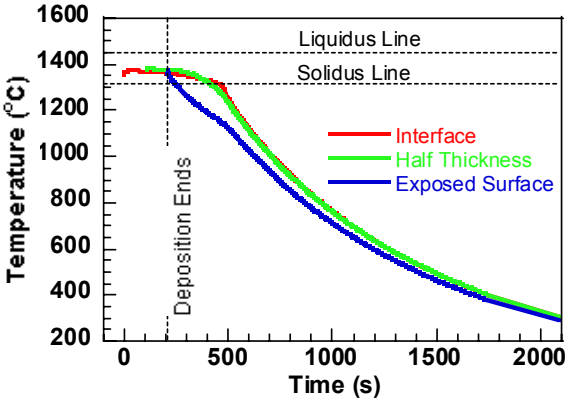

Fig. 5

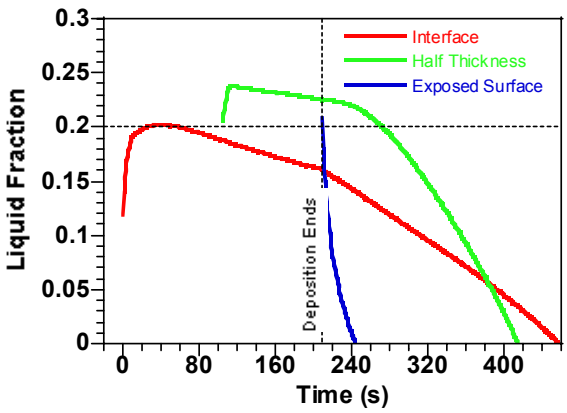

Fig. 6

Fig. 5: Calculated temperature as a function of time in spray-formed H13 tooling.
Fig. 6: Calculated liquid fraction as a function of time in spray-formed H13 tooling.

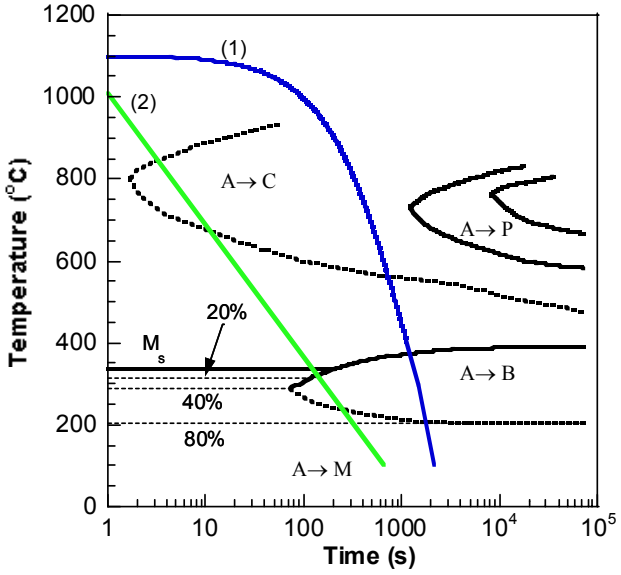

(1): Calculated cooling curve

(2): Average cooling curve during conventional air quenching [15]

A: austenite
C: carbides
P: pearlite
B: binite
M: martensite

Fig. 7: The prediction of phases in as-deposited H13

In order to predict the phases in the as-spray-formed H13, the region representing a temperature lower than 1100 °C in the calculated curve of temperature vs. time is mapped to the transformation diagram of H13 steel [14], as shown in Fig. 7. It is noted that austenite decomposition occurs only when the temperature deceases to a value that is lower than the temperature corresponding to the austenite single-phase region in the equilibrium phase

diagram of H13. The lowest temperature corresponding to the austenite single-phase region is estimated to be 1100 °C [14]. On the basis of the prediction in Fig. 7, as-spray-formed H13 consists of proeutectoid carbides, bainite, martensite and retained austenite, consistent with the aforementioned SEM (Fig. 2b) and TEM (Figs. 3 and 4) observations.

The higher hardness values of spray-formed H13 as compared to those of conventionally heat-treated H13 can also be rationalized on the basis of Fig. 7. In order to do this, the average cooling curve during conventional air quenching [15] is shown overlapping the transformation diagram of H13 in Fig. 7. During spray forming of H13 tooling, austenite decomposition starts from the austenite single-phase region, while in conventional quenching of H13 it starts from the phase region containing austenite and carbides [14]. As a result, more alloying elements and carbon are dissolved in the matrix of spray-formed H13 tooling. However, the cooling rate in spray-formed H13 is slower than that in conventional quenching of H13 (Fig.7), leading to more precipitation of alloying elements and carbon in the form of carbides. By combing the two factors, the former factor overwhelms the latter factor, leading to a higher aging hardness in spray-formed H13 tooling as shown in Table III.

Acknowledgements

The authors would like to acknowledge the financial support from the United States Department of Energy (FWP Number 42C5-05).

References

1. E. J. Lavernia and Y. Wu, Spray atomization and deposition, (John Wiley & Sons, Inc., New York, NY, 1996).
2. K. M. McHugh, "Spray-formed tooling and aluminum strip", in P/M in Aerospace, Defense and Demanding Applications-1995, ed. F. H. Froes, (Metal Powder Industries Federation, Princeton, NJ, 1995), pp. 345-353.
3. K. M. McHugh, "Microstructure transformation of spray-formed H13 tool steel during deposition and heat treatment", in Solidification 1998, the proceedings of a symposium in 1998 TMS Annual meeting, ed. S. P. Marsh et al., (TMS, Warrendale, PA, 1998), pp. 427-438.
4. E. S. Lee et al., "Different carbide types and their effect on bend properties of a spray-formed high speed steel", Scripta Materialia, 39 (1998), pp. 1133-1138.
5. J. R. Knirsch, "Spray forming, rapid solidification process-an update", in Proceedings of 2001 International Die Casting Congress, Oct. 29-Nov. 1, Cincinnati, Ohio.
6. B. C. Moon et al., "In situ temperature measurement during spray forming of A2-tool steel and axisymmetric two-dimensional analysis", J. Mater. Res., 15 (2000), pp.1669-1678.
7. Crucible Tool Co., Private communication, 2004.
8. Q. Xu and E. J. Lavernia, "Influence of nucleation and growth phenomena on microstructural evolution during droplet-based deposition", Acta Mater., 49(2001), pp.3849-3861.
9. K. Lubanska, "Correlation of spray ring data for gas atomization of liquid metals", J. Met., 22 (Feb.) (1970), pp. 45-49.
10. P. S. Grant, B. Cantor and L. Katgerman, "Modeling of droplet dynamic and thermal histories during spray forming. 2. effect of process parameters", Acta Metall. Mater., 41 (1993), pp. 3109-3118.
11. Q. Xu, V. V. Gupta and E. J. Lavernia, "On the mechanism of mushy layer formation during droplet-based processing", Metall. Mater. Trans. B, 30B (1999), pp. 527-539.
12. Source Book on Industrial Alloy and Engineering Data, (American Society for Metals, Materials Park, OH, 1978), p. 267.
13. S. Annavarapu and R. Doherty, "Evolution of microstructure in spray casting", Int. J. Powder Metall., 29 (1993), pp. 331-343.
14. G. A. Roberts, and R. A. Cary, Tool Steels, (American Society for Metals, Materials Park, OH, 1980), pp. 563-625.
15. Metal Handbook (9th edition), vol.4: Heat Treating, (American Society for Metals, Materials Park, OH, 1981), p.59.